Journal of Molecular Catalysis A: Chemical 319 (2010) 98–107

Contents lists available at ScienceDirect

Journal of Molecular Catalysis A: Chemical

journal homepage: www.elsevier.com/locate/molcata

Direct synthesis of hydrogen peroxide from hydrogen and oxygen over palladium catalyst supported on SO_3H-functionalized mesoporous silica

Sunyoung Park[a], Sung-Hyeon Baeck[b], Tae Jin Kim[c], Young-Min Chung[c], Seung-Hoon Oh[c], In Kyu Song[a,*]

[a] School of Chemical and Biological Engineering, Institute of Chemical Processes, Seoul National University, Shinlim-dong, Kwanak-ku, Seoul 151-744, South Korea
[b] Department of Chemical Engineering, Inha University, Inchon 402-751, South Korea
[c] SK Energy Corporation, Yuseong-ku, Daejeon 305-712, South Korea

ARTICLE INFO

Article history:
Received 26 September 2009
Received in revised form 9 December 2009
Accepted 12 December 2009
Available online 22 December 2009

Keywords:
Hydrogen peroxide
Hydrogen
Oxygen
SO_3H-functionalized mesoporous silica
Palladium

ABSTRACT

Palladium catalysts supported on SO_3H-functionalized mesoporous silicas (denoted as Pd/SO_3H-MCM-41, Pd/SO_3H-MCM-48, Pd/SO_3H-MSU-1, Pd/SO_3H-SBA-15, and Pd/SO_3H-MCF) were applied to the direct synthesis of hydrogen peroxide from hydrogen and oxygen. For comparison, palladium catalysts supported on mesoporous silicas (denoted as Pd/MCM-41, Pd/MCM-48, Pd/MSU-1, Pd/SBA-15, and Pd/MCF) were also employed for the direct synthesis of hydrogen peroxide. Selectivity for hydrogen peroxide, yield for hydrogen peroxide, and final concentration of hydrogen peroxide over Pd/SO_3H-functionalized mesoporous silica catalysts were much higher than those over Pd/mesoporous silica catalysts. Yield for hydrogen peroxide increased with increasing acid density of Pd/SO_3H-functionalized mesoporous silica. Pd/SO_3H-functionalized mesoporous silicas efficiently served as an alternate acid source and as an active metal catalyst in the direct synthesis of hydrogen peroxide from hydrogen and oxygen.

1. Introduction

Hydrogen peroxide (H_2O_2) has been widely utilized in many areas such as pulp industry, textile industry, and wastewater treatment [1,2]. Hydrogen peroxide has also been used as a clean and strong oxidant in the epoxidation of propylene to propylene oxide [3]. Hydrogen peroxide currently available in the market is mostly produced through the anthraquinone process [1,2]. However, the anthraquinone process uses toxic solvents and requires many energy intensive steps for purification of hydrogen peroxide [1,2]. Therefore, direct synthesis of hydrogen peroxide from hydrogen and oxygen has attracted much attention as an economical and environmentally benign process [4–17].

In the direct synthesis of hydrogen peroxide from hydrogen and oxygen, several undesired reactions occur simultaneously together with selective oxidation of hydrogen to hydrogen peroxide (reaction 1) (Fig. 1) [1,2]. These undesired reactions include formation of water (reaction 2), hydrogenation of hydrogen peroxide (reaction 3), and decomposition of hydrogen peroxide (reaction 4). All these reactions are thermodynamically favorable and highly exothermic. Especially, formation of water and hydrogenation of hydrogen peroxide are thermodynamically more favorable than selective oxidation of hydrogen to hydrogen peroxide. Consequently, selectivity for hydrogen peroxide in the direct synthesis of hydrogen peroxide is limited by these undesired reactions. Therefore, many attempts have been made to increase the selectivity for hydrogen peroxide in the direct synthesis of hydrogen peroxide [7–11].

A large number of noble metals such as palladium [4–11], gold [12], palladium–gold [13–16], and palladium–platinum [16,17] have been used as catalysts in the direct synthesis of hydrogen peroxide from hydrogen and oxygen. Among these catalysts, palladium has been widely investigated as an efficient catalyst for the direct synthesis of hydrogen peroxide [4–11]. Palladium catalysts have been supported on various materials such as alumina, silica, and carbon for effective dispersion of active metal component [6].

Acids and halides have been used as additives to enhance the selectivity for hydrogen peroxide in the direct synthesis of hydrogen peroxide from hydrogen and oxygen [7–11]. It is known that acids prevent the decomposition of hydrogen peroxide and halides inhibit the formation of water [1,2]. However, acid additives cause the dissolution of active metal component from the supported catalyst and accelerate the corrosion of reactor [1,2]. Therefore, acidic solid supports have been employed for the direct synthesis of hydrogen peroxide in order to minimize the amount of acid additives [18–21].

It is known that SO_3H-functionalized mesoporous silicas have excellent acid property [22,23]. Therefore, SO_3H-functionalized mesoporous silicas have been used as solid acid catalysts in several

* Corresponding author. Tel.: +82 2 880 9227; fax: +82 2 889 7415.
E-mail address: inksong@snu.ac.kr (I.K. Song).

1381-1169/$ – see front matter © 2009 Elsevier B.V. All rights reserved.
doi:10.1016/j.molcata.2009.12.006

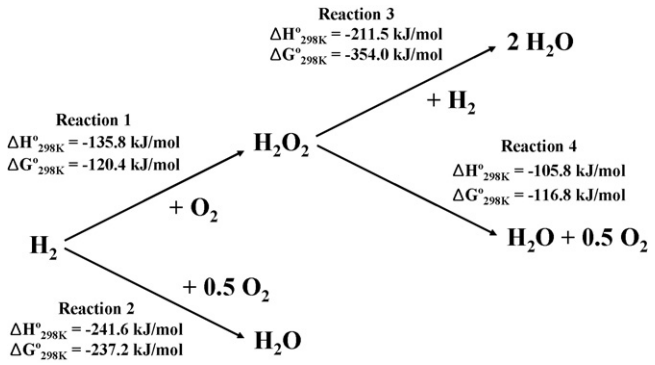

Fig. 1. Reactions involved in the direct synthesis of hydrogen peroxide from hydrogen and oxygen.

acid-catalyzed reactions such as esterification and condensation [22,23]. Furthermore, an enhanced catalytic performance of palladium catalyst supported on SO_3H-functionalized SBA-15 was observed in the direct synthesis of hydrogen peroxide from hydrogen and oxygen in our previous work [21].

Mesoporous silicas have been utilized in many fields of science and engineering, including catalysis, adsorption, and separation, because they have uniform pore size, high surface area, and large pore volume [24–29]. It has been reported that mesoporous silicas formed by different templating agent exhibit different pore size, pore structure, and amount of surface hydroxyl group [24–29]. Therefore, it is expected that SO_3H-functionalized mesoporous silicas with different acid and physical properties will show a different catalytic activity in the direct synthesis of hydrogen peroxide.

In this work, palladium catalysts supported on SO_3H-functionalized mesoporous silicas were prepared using MCM-41, MCM-48, MSU-1, SBA-15, and MCF. They were then applied to the direct synthesis of hydrogen peroxide from hydrogen and oxygen, with an aim of utilizing palladium and SO_3H-functionalized mesoporous silica as an active metal component and as an alternate acid source, respectively. The effect of SO_3H functionalization of mesoporous silica support on the catalytic performance of supported palladium catalyst in the direct synthesis of hydrogen peroxide was investigated.

2. Experimental

2.1. Catalyst preparation

MCM-41, MCM-48, MSU-1, SBA-15, and MCF were selected as mesoporous silica materials. MCM-41 was purchased from Sigma–Aldrich. MCM-48, MSU-1, SBA-15, and MCF were synthesized according to the reported methods [24–29]. SO_3H-functionalized mesoporous silica was prepared by a grafting method, according to the similar method reported in literatures [30,31]. SO_3H-functionalized mesoporous silica supports were denoted as SO_3H-MCM-41, SO_3H-MCM-48, SO_3H-MSU-1, SO_3H-SBA-15, and SO_3H-MCF. Palladium catalyst supported on SO_3H-functionalized mesoporous silica was then prepared by an ion-exchange method. Palladium catalysts supported on SO_3H-functionalized mesoporous silicas (Pd/SO_3H-functionalized mesoporous silicas) were denoted as Pd/SO_3H-MCM-41, Pd/SO_3H-MCM-48, Pd/SO_3H-MSU-1, Pd/SO_3H-SBA-15, and Pd/SO_3H-MCF.

Fig. 2 shows the schematic procedures for the preparation of Pd/SO_3H-functionalized mesoporous silica. For example, typical procedures for the preparation of Pd/SO_3H-MCM-41 catalyst are as follows. MCM-41 was dispersed in anhydrous toluene (Sigma–Aldrich) with constant stirring under nitrogen atmosphere. After adding 3-mercaptopropyltrimethoxy silane (3-MPTMS, Sigma–Aldrich) into the dispersed solution, the mixture was stirred for 1 day. A solid recovered from the mixture by filtration was washed with toluene, and then it was dried overnight at 80 °C. Thiol (–SH) group on the surface of MCM-41 was converted into sulfonic acid ($–SO_3H$) group by treating the solid with an aqueous solution of HNO_3. For this, the solid was dispersed in 20% HNO_3 solution, and subsequently, 69% HNO_3 solution was

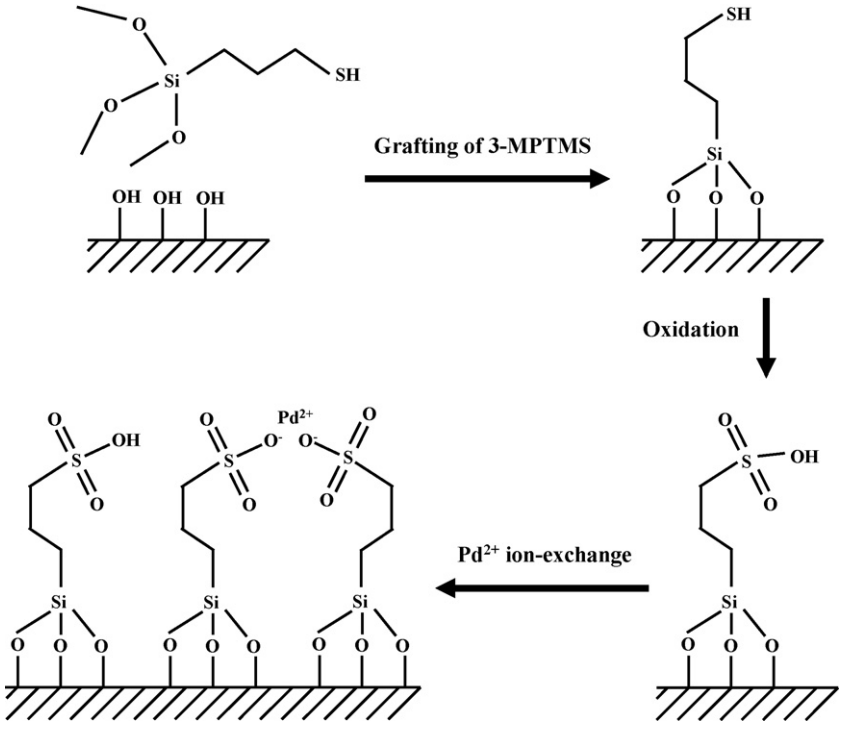

Fig. 2. Schematic procedures for the preparation of Pd/SO_3H-functionalized mesoporous silica.

slowly added. The mixture was stirred for 1 day at room temperature. After washing the resulting solid with distilled water, the solid was dried overnight at 80 °C to obtain SO_3H-MCM-41 support. SO_3H-MCM-41 was added to an aqueous solution of $Pd(NO_3)_2$ (Sigma–Aldrich) with constant stirring. A solid product recovered by filtration was washed with distilled water, and then it was dried overnight at 80 °C to yield Pd/SO_3H-MCM-41 catalyst. The preparation procedures for Pd/SO_3H-MCM-48, Pd/SO_3H-MSU-1, Pd/SO_3H-SBA-15, and Pd/SO_3H-MCF catalysts were almost identical to those for Pd/SO_3H-MCM-41 catalyst. The Pd loading was fixed at 0.5 wt% in all cases.

For comparison, palladium catalyst supported on mesoporous silica was prepared by an incipient wetness method. The impregnated catalyst was dried overnight at 80 °C, and then it was calcined at 500 °C for 3 h to convert palladium nitrate into palladium oxide. The palladium loading was also fixed at 0.5 wt%. The prepared palladium catalysts supported on mesoporous silicas (Pd/mesoporous silicas) were denoted as Pd/MCM-41, Pd/MCM-48, Pd/MSU-1, Pd/SBA-15, and Pd/MCF.

2.2. Catalyst characterization

Pore structure and pore size of materials were examined by TEM analysis (Jeol, JEM-3000F). N_2 adsorption–desorption isotherm was obtained with an ASAP-2010 instrument (Micromeritics), and pore size distribution was determined by the BJH (Barret–Joyner–Hallender) method applied to the desorption branch of the isotherm. Small angle X-ray scattering (SAXS) experiment (Bruker, GADDS) was performed in order to confirm the mesoporous structure of silica materials. Crystalline phase of the catalyst was confirmed by XRD measurement (Rigaku, D-Max2500-PC) using Cu Kα radiation operated at 50 kV and 100 mA. Palladium content of the catalyst before and after the reaction was measured by ICP-AES analysis (PerkinElmer, Optima-4300 DV). Chemical state of SO_3H-functionalized mesoporous silica was examined by ^{13}C CP-MAS NMR analysis (Bruker, AVANCE 400 WB) to ensure the successful grafting of $–SO_3H$ group on the surface of mesoporous silica [30–32]. Acid–base titration [33,34] was carried out in order to measure the acid amount of catalyst. In a typical measurement, 0.3 g of catalyst was dispersed in 30 ml of 0.1 M KCl solution. The mixture was stirred for 20 min and then titrated with 0.2 M KOH solution in the presence of phenolphthalein.

2.3. Direct synthesis of hydrogen peroxide

Direct synthesis of hydrogen peroxide from hydrogen and oxygen was carried out in an autoclave reactor in the absence of acid additive. 80 ml of methanol and 1.0 g of each catalyst were charged into the reactor. Sodium bromide (6.32 mg) was then added as a halide additive. H_2/N_2 (25 mol% H_2) and O_2/N_2 (50 mol% O_2) were bubbled through the reaction medium under vigorous stirring (1000 rpm). H_2/O_2 ratio in the feed stream was fixed at 0.4, and total feed rate was maintained at 44 ml/min. Catalytic reaction was carried out at 28 °C and 10 atm for 6 h. In order to solve the safety problem, mixed gases diluted with an inert gas (H_2/N_2 (25 mol% H_2) and O_2/N_2 (50 mol% O_2)) and an autoclave reactor equipped with a flashback arrestor as well as a safety valve were used in the direct synthesis of hydrogen peroxide. Unreacted hydrogen was analyzed using a gas chromatograph (Younglin, ACME 6000) equipped with a TCD. Concentration of hydrogen peroxide was determined by an iodometric titration method [35]. Conversion of hydrogen and selectivity for hydrogen peroxide were calculated according to the following equations. Yield for hydrogen peroxide was calculated by multiplying conversion of hydrogen and selectivity for hydrogen peroxide:

$$\text{conversion of hydrogen} = \frac{\text{moles of hydrogen reacted}}{\text{moles of hydrogen supplied}}$$

$$\text{selectivity for hydrogen peroxide} = \frac{\text{moles of hydrogen peroxide formed}}{\text{moles of hydrogen reacted}}$$

2.4. Hydrogenation of hydrogen peroxide

Hydrogenation of hydrogen peroxide was carried out in an autoclave reactor containing 80 ml of methanol, 1.0 g of each catalyst, and 6.32 mg of sodium bromide. 3 ml of 30 wt% hydrogen peroxide was added into the reactor. H_2/N_2 (25 mol% H_2) and N_2 were bubbled through the reaction medium under vigorous stirring (1000 rpm). H_2/N_2 ratio in the feed stream was fixed at 0.1, and total feed rate was maintained at 44 ml/min. The reaction was carried out at 28 °C and 10 atm for 6 h. Concentration of hydrogen peroxide was determined by an iodometric titration method [35]. Degree of hydrogenation of H_2O_2 was calculated according to the following equation:

$$\text{degree of hydrogenation of } H_2O_2 = \frac{\text{moles of hydrogen peroxide hydrogenated}}{\text{moles of hydrogen peroxide supplied}}$$

2.5. Decomposition of hydrogen peroxide

Decomposition of hydrogen peroxide was carried out in an autoclave reactor containing 80 ml of methanol, 1.0 g of each catalyst, and 6.32 mg of sodium bromide. 3 ml of 30 wt% hydrogen peroxide was added into the reactor. N_2 (44 ml/min) was bubbled through the reaction medium under vigorous stirring (1000 rpm). The reaction was carried out at 28 °C and 10 atm for 6 h. Concentration of hydrogen peroxide was determined by an iodometric titration method [35]. Degree of decomposition of H_2O_2 was calculated according to the following equation:

$$\text{degree of decomposition of } H_2O_2 = \frac{\text{moles of hydrogen peroxide decomposed}}{\text{moles of hydrogen peroxide supplied}}$$

3. Results and discussion

3.1. Physical property of mesoporous silica and supported palladium catalyst

Fig. 3 shows the TEM images of mesoporous silicas (MCM-41, MCM-48, MSU-1, SBA-15, and MCF). MCM-41 showed a hexagonal pore structure consisting of 1-dimensional rod-like pores. MCM-48 exhibited a 3-dimensional pore structure, and MSU-1 had a wormhole-like pore structure. Pore sizes of MCM-41, MCM-48, and MSU-1 determined from TEM images were ca. 2 nm. Pore structure of SBA-15 was similar to that of MCM-41, but pore size of SBA-15 was ca. 4 nm. MCF exhibited a disordered pore structure with large pores in the range of 8–10 nm. Pore structures and pore sizes of mesoporous silicas were in good agreement with those reported in literatures [24–29], indicating successful preparation of mesoporous silicas.

Fig. 4 shows the TEM images of Pd/SO_3H-functionalized mesoporous silicas (Pd/SO_3H-MCM-41, Pd/SO_3H-MCM-48, Pd/SO_3H-MSU-1, Pd/SO_3H-SBA-15, and Pd/SO_3H-MCF). Pore structure and

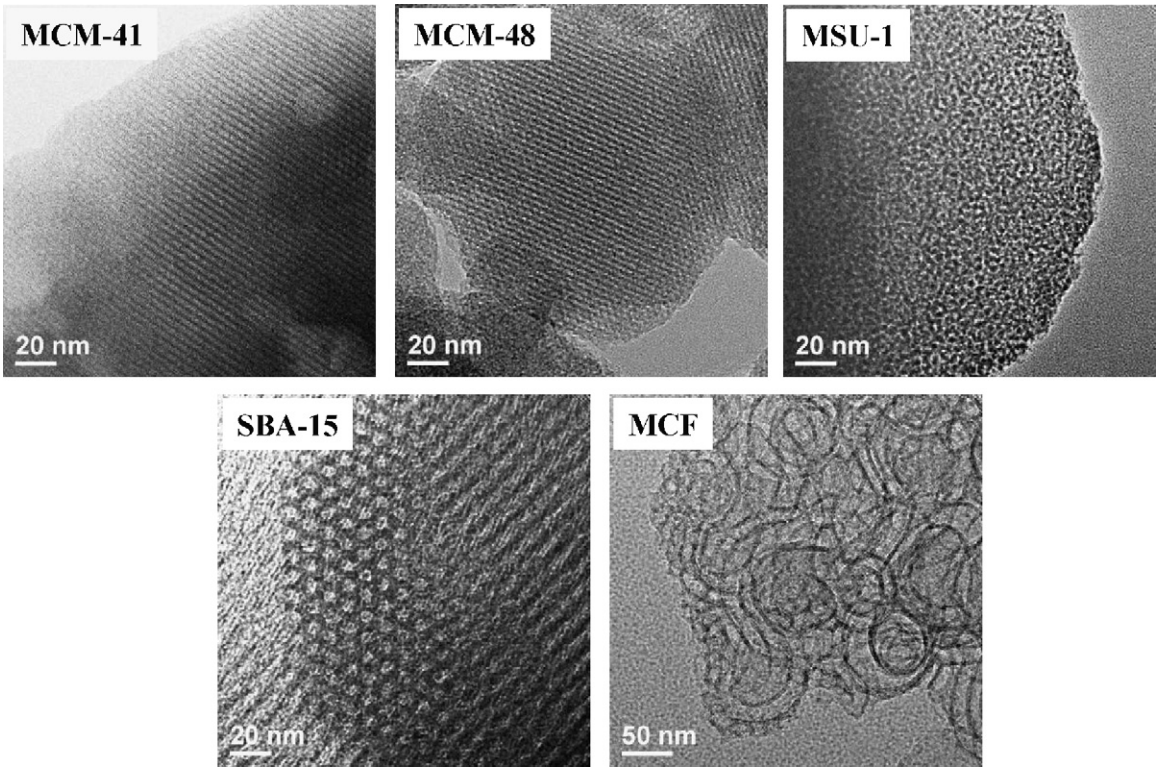

Fig. 3. TEM images of mesoporous silicas (MCM-41, MCM-48, MSU-1, SBA-15, and MCF).

pore size of Pd/SO_3H-functionalized mesoporous silica were almost identical to those of corresponding mesoporous silica, indicating that pore structure of mesoporous silica was still maintained even after the SO_3H functionalization and subsequent Pd loading. Furthermore, no visible evidence representing palladium particles was observed in the TEM images of Pd/SO_3H-functionalized mesoporous silicas. This implies that palladium species were finely dispersed on the surface of SO_3H-functionalized mesoporous silicas, as illustrated in Fig. 2.

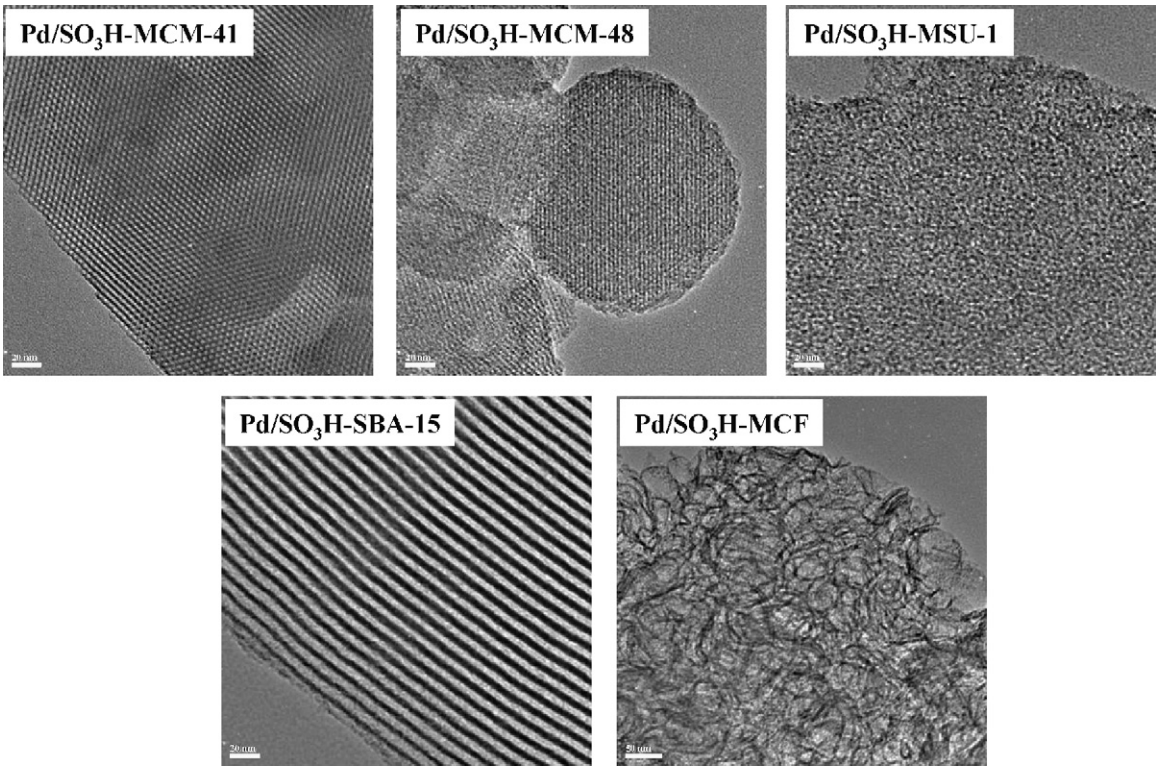

Fig. 4. TEM images of Pd/SO_3H-functionalized mesoporous silicas (Pd/SO_3H-MCM-41, Pd/SO_3H-MCM-48, Pd/SO_3H-MSU-1, Pd/SO_3H-SBA-15, and Pd/SO_3H-MCF).

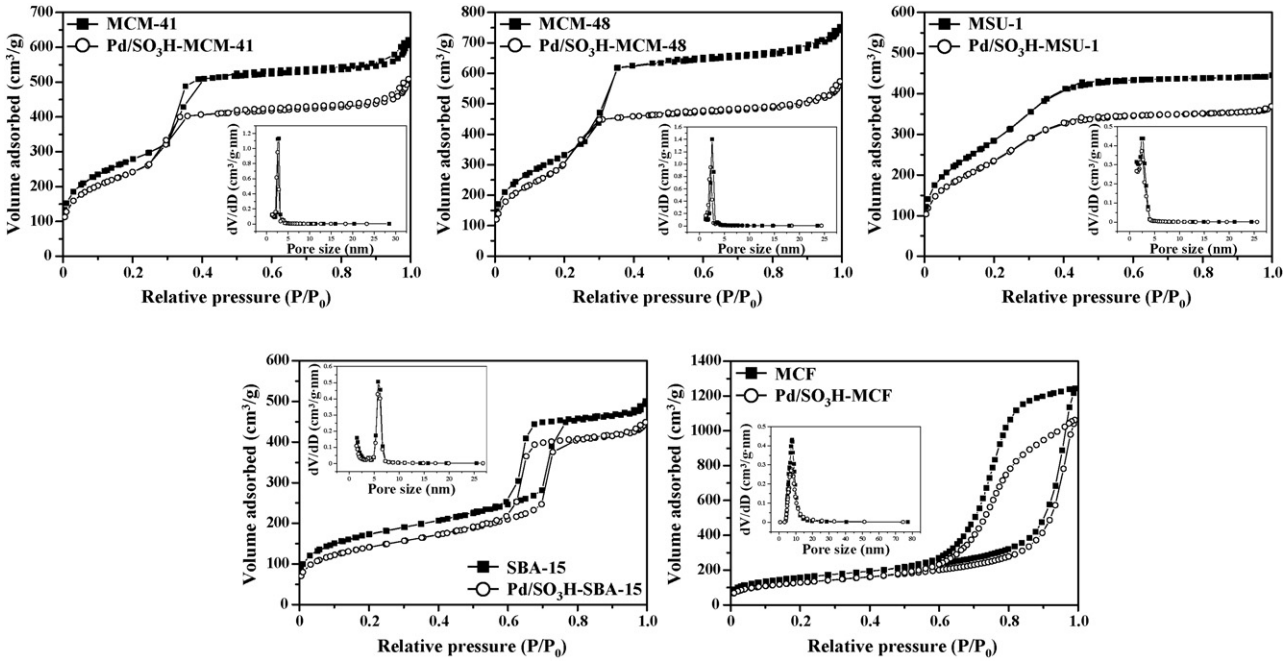

Fig. 5. N_2 adsorption–desorption isotherms and pore size distributions of mesoporous silicas (MCM-41, MCM-48, MSU-1, SBA-15, and MCF) and Pd/SO_3H-functionalized mesoporous silicas (Pd/SO_3H-MCM-41, Pd/SO_3H-MCM-48, Pd/SO_3H-MSU-1, Pd/SO_3H-SBA-15, and Pd/SO_3H-MCF).

Fig. 5 shows the N_2 adsorption–desorption isotherms and pore size distributions of mesoporous silicas (MCM-41, MCM-48, MSU-1, SBA-15, and MCF). It was observed that MCM-41, MCM-48, and MSU-1 exhibited IV-type isotherms without hysteresis, while SBA-15 and MCF showed IV-type isotherms with H1-type hysteresis loops, as reported in the previous works [26–29,36]. Detailed textural properties of mesoporous silicas are summarized in Table 1. Pore sizes of mesoporous silicas were in agreement with those determined by TEM analyses. These results also support that mesoporous silicas were successfully prepared in this work.

N_2 adsorption–desorption isotherms and pore size distributions of Pd/SO_3H-functionalized mesoporous silicas (Pd/SO_3H-MCM-41, Pd/SO_3H-MCM-48, Pd/SO_3H-MSU-1, Pd/SO_3H-SBA-15, and Pd/SO_3H-MCF) are also shown in Fig. 5. Pd/SO_3H-functionalized mesoporous silica exhibited almost the same N_2 adsorption–desorption isotherm and pore size distribution as corresponding mesoporous silica. This indicates that pore structures of mesoporous silicas were still maintained even after the grafting of –SO_3H group on the surface of mesoporous silicas. Detailed textural properties of Pd/SO_3H-functionalized mesoporous silicas are summarized in Table 1. It was observed that surface area and pore volume of Pd/SO_3H-functionalized mesoporous silica were lower than those of corresponding mesoporous silica due to the grafting of –SO_3H group. However, Pd/SO_3H-functionalized mesoporous silicas still retained high surface areas and large pore volumes.

Table 1
Surface area, pore volume, and average pore size of mesoporous silica and Pd/SO_3H-functionalized mesoporous silica.

	Surface area (m^2/g)[a]	Pore volume (cm^3/g)[b]	Average pore size (nm)[c]
MCM-41	1013	0.94	2.7
MCM-48	1222	1.14	2.5
MSU-1	1059	0.75	2.2
SBA-15	622	0.76	4.4
MCF	559	1.93	8.0
Pd/SO_3H-MCM-41	880	0.74	2.5
Pd/SO_3H-MCM-48	1121	0.86	2.2
Pd/SO_3H-MSU-1	872	0.61	2.2
Pd/SO_3H-SBA-15	508	0.67	4.6
Pd/SO_3H-MCF	459	1.65	8.8

[a] Calculated by the BET (Brunauer–Emmett–Teller) equation.
[b] BJH (Barret–Joyner–Hallender) desorption pore volume.
[c] BJH (Barret–Joyner–Hallender) desorption average pore diameter.

Fig. 6 shows the small angle X-ray scattering (SAXS) patterns of mesoporous silicas (MCM-41, MCM-48, MSU-1, SBA-15, and MCF) and Pd/SO_3H-functionalized mesoporous silicas (Pd/SO_3H-MCM-41, Pd/SO_3H-MCM-48, Pd/SO_3H-MSU-1, Pd/SO_3H-SBA-15, and Pd/SO_3H-MCF). SAXS patterns of mesoporous silicas were in good agreement with those reported in literatures [24–29]. This indicates that mesoporous silicas were successfully prepared in this work, as also evidenced by TEM images and N_2 adsorption–desorption isotherms. SAXS pattern of Pd/SO_3H-functionalized mesoporous silica was almost identical to that of corresponding mesoporous silica. This result also supports that pore structures of mesoporous silicas were still maintained even after the grafting of –SO_3H group and subsequent Pd loading.

Fig. 7 shows the XRD patterns of Pd/SO_3H-functionalized mesoporous silicas (Pd/SO_3H-MCM-41, Pd/SO_3H-MCM-48, Pd/SO_3H-MSU-1, Pd/SO_3H-SBA-15, and Pd/SO_3H-MCF). For comparison, XRD patterns of Pd/mesoporous silicas (Pd/MCM-41, Pd/MCM-48, Pd/MSU-1, Pd/SBA-15, and Pd/MCF) are also shown in Fig. 7. No characteristic diffraction peak for PdO (JCPDS 43-1024) was observed in the Pd/SO_3H-functionalized mesoporous silicas. However, Pd/mesoporous silicas exhibited a weak diffraction peak corresponding to PdO. These results indicate that palladium species were finely dispersed on the surface of SO_3H-functionalized mesoporous silicas, as also demonstrated by TEM images (Fig. 4).

3.2. Grafting of –SO_3H functional group

Fig. 8 shows the ^{13}C CP-MAS NMR spectra of SO_3H-functionalized mesoporous silica supports (SO_3H-MCM-41, SO_3H-MCM-48, SO_3H-MSU-1, SO_3H-SBA-15, and SO_3H-MCF). All the SO_3H-functionalized mesoporous silica supports showed three resonance peaks at δ = 11.2 (C^1) ppm, 18.3 (C^2) ppm, and 54.1 (C^3) ppm. These resonance peaks were attributed to different carbon atoms

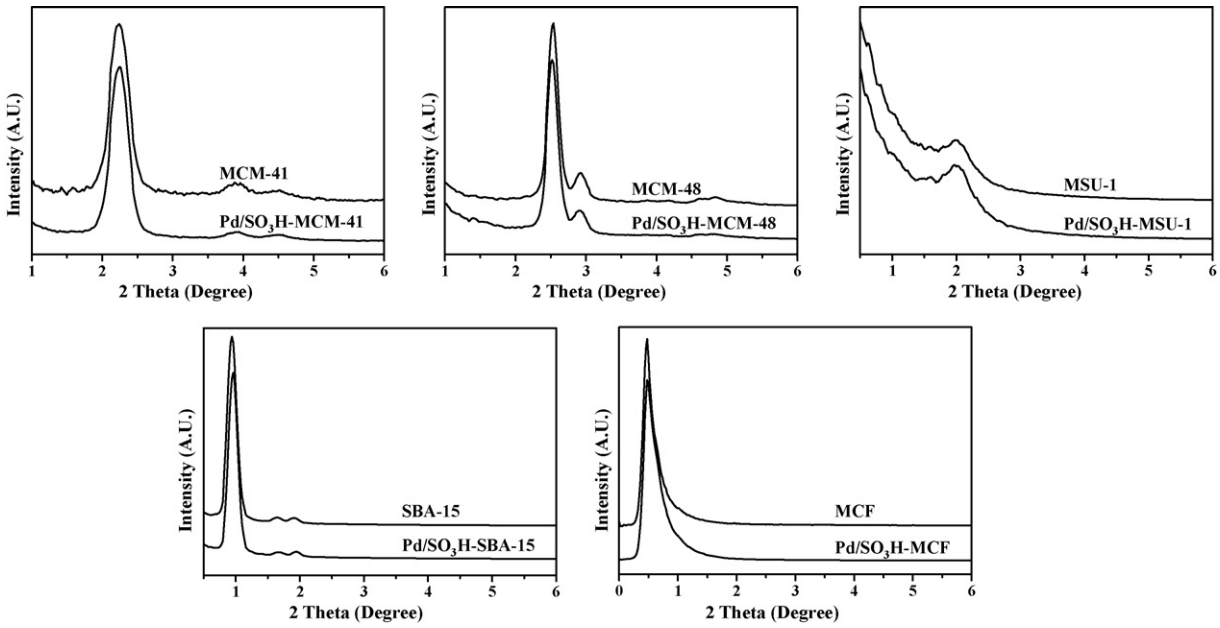

Fig. 6. Small angle X-ray scattering (SAXS) patterns of mesoporous silicas (MCM-41, MCM-48, MSU-1, SBA-15, and MCF) and Pd/SO_3H-functionalized mesoporous silicas (Pd/SO_3H-MCM-41, Pd/SO_3H-MCM-48, Pd/SO_3H-MSU-1, Pd/SO_3H-SBA-15, and Pd/SO_3H-MCF).

in 3-MPTMS; C^1 carbon directly bonded to Si atom, C^2 carbon of propyl chain, and C^3 carbon bonded to –SO_3H group [30–32]. It should be noted that no characteristic peak was observed at around 29 ppm in all the samples. This indicates that –SH group was completely converted to –SO_3H group during the surface oxidation step [30,32]. Moreover, any peaks were not detected at 40 ppm and 23 ppm. This implies that no disulfide species were formed under our preparation conditions [37]. The above results indicate that –SO_3H group was successfully grafted on the surface of mesoporous silica.

3.3. Catalytic performance in the direct synthesis of hydrogen peroxide

Fig. 9 shows the catalytic performance of Pd/mesoporous silicas (Pd/MCM-41, Pd/MCM-48, Pd/MSU-1, Pd/SBA-15, and Pd/MCF)

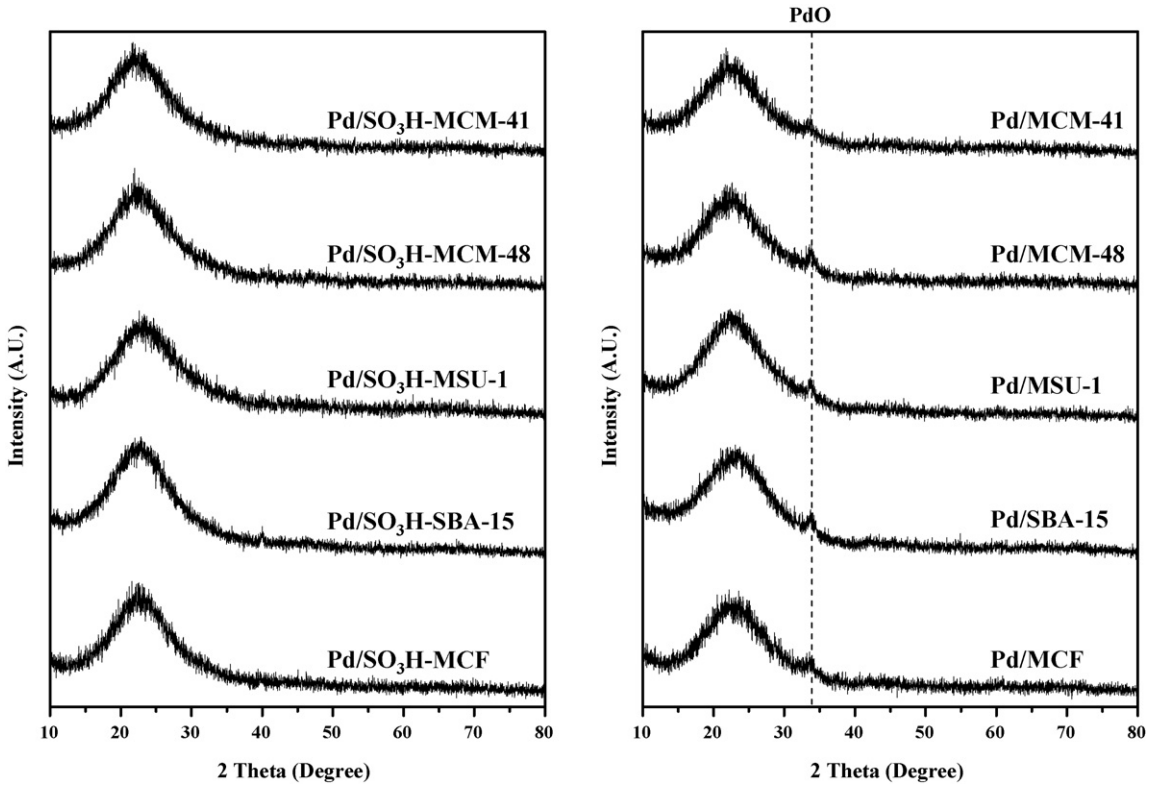

Fig. 7. XRD patterns of Pd/SO_3H-functionalized mesoporous silicas (Pd/SO_3H-MCM-41, Pd/SO_3H-MCM-48, Pd/SO_3H-MSU-1, Pd/SO_3H-SBA-15, and Pd/SO_3H-MCF) and Pd/mesoporous silicas (Pd/MCM-41, Pd/MCM-48, Pd/MSU-1, Pd/SBA-15, and Pd/MCF).

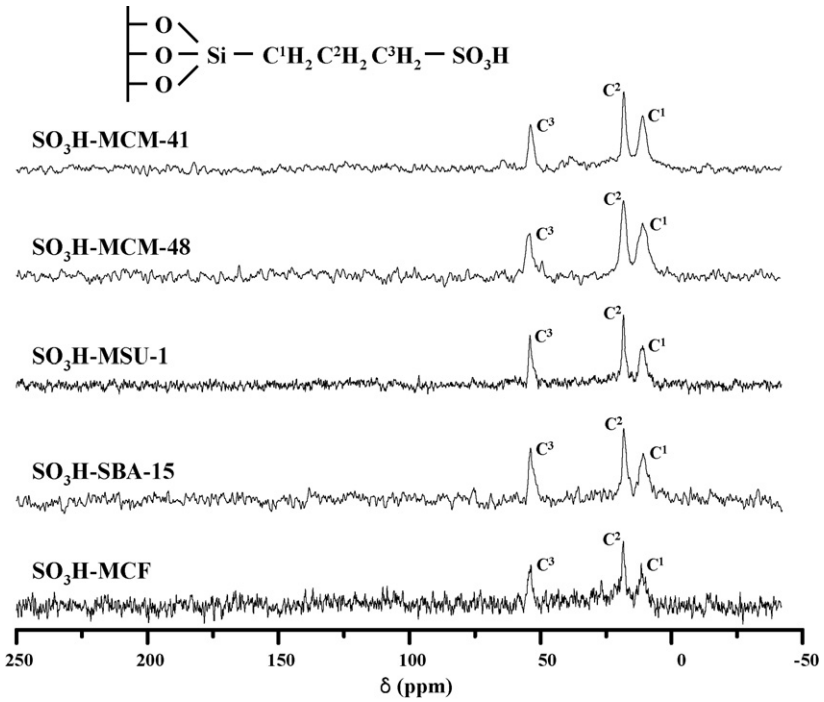

Fig. 8. ^{13}C CP-MAS NMR spectra of SO_3H-functionalized mesoporous silica supports (SO_3H-MCM-41, SO_3H-MCM-48, SO_3H-MSU-1, SO_3H-SBA-15, and SO_3H-MCF).

in the direct synthesis of hydrogen peroxide from hydrogen and oxygen. Conversion of hydrogen over Pd/mesoporous silica catalysts was high. However, yield for hydrogen peroxide over Pd/mesoporous silica catalysts was very low, because selectivity for hydrogen peroxide over the catalysts was extremely low. Final concentration of hydrogen peroxide after a 6-h reaction over Pd/mesoporous silica catalysts was less than 0.1 wt%. This indicates that undesired reactions such as formation of water and decomposition of hydrogen peroxide were also activated over Pd/mesoporous silica catalysts [1,2]. It is noteworthy that yield for hydrogen peroxide over Pd/mesoporous silica catalysts was in the range of 0.6–1.4% with no great difference.

Fig. 10 shows the catalytic performance of Pd/SO_3H-functionalized mesoporous silicas (Pd/SO_3H-MCM-41, Pd/SO_3H-MCM-48, Pd/SO_3H-MSU-1, Pd/SO_3H-SBA-15, and Pd/SO_3H-MCF) in the direct synthesis of hydrogen peroxide from hydrogen and oxygen. Conversion of hydrogen over Pd/SO_3H-functionalized mesoporous silica catalysts was lower than that over Pd/mesoporous silica catalysts. However, selectivity and yield for hydrogen peroxide over Pd/SO_3H-functionalized mesoporous silica catalysts were much higher than those over Pd/mesoporous silica catalysts. Furthermore, final concentration of hydrogen peroxide after a 6-h reaction over Pd/SO_3H-functionalized mesoporous silica catalysts was much higher than that over Pd/mesoporous silica catalysts. This implies that Pd/SO_3H-functionalized mesoporous silica catalysts enhanced the selectivity for hydrogen peroxide by preventing the decomposition of hydrogen peroxide. As mentioned earlier, it is known that acid additives prevent the decomposition of hydrogen peroxide [1,2]. It has been reported that the dissociation of hydrogen peroxide ($H_2O_2 \Leftrightarrow HO_2^- + H^+$) is suppressed when hydrogen peroxide is surrounded by protons (H^+ ions) of acid additives [1,2]. Therefore, it can be inferred that the improved selectivity for hydrogen peroxide over Pd/SO_3H-functionalized mesoporous silica catalysts was attributed to the enhanced acid property of Pd/SO_3H-functionalized mesoporous silica catalysts, as reported in our previous works [20,21].

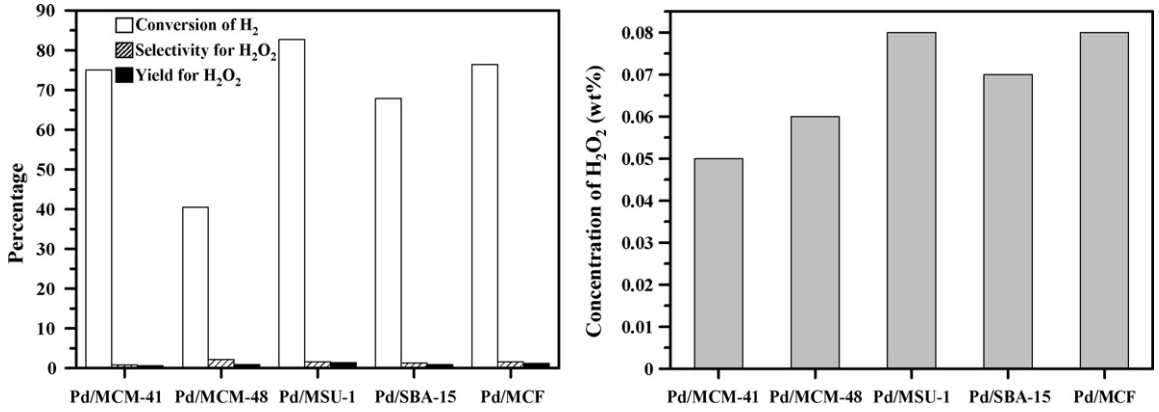

Fig. 9. Catalytic performance of Pd/mesoporous silicas (Pd/MCM-41, Pd/MCM-48, Pd/MSU-1, Pd/SBA-15, and Pd/MCF) in the direct synthesis of hydrogen peroxide from hydrogen and oxygen.

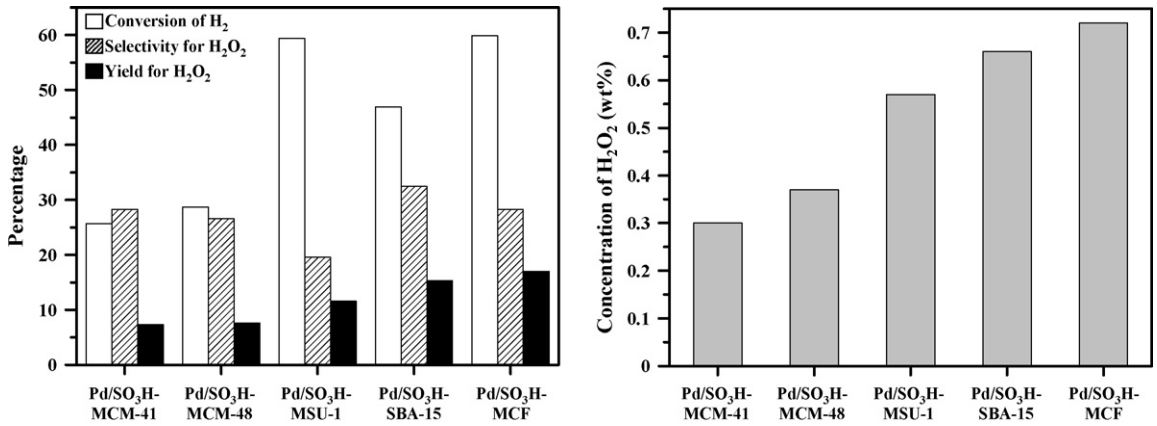

Fig. 10. Catalytic performance of Pd/SO_3H-functionalized mesoporous silicas (Pd/SO_3H-MCM-41, Pd/SO_3H-MCM-48, Pd/SO_3H-MSU-1, Pd/SO_3H-SBA-15, and Pd/SO_3H-MCF) in the direct synthesis of hydrogen peroxide from hydrogen and oxygen.

Table 2
Palladium content of Pd/SO_3H-functionalized mesoporous silica before and after the direct synthesis of hydrogen peroxide from hydrogen and oxygen.

Catalyst	Palladium content (wt%)	
	Before reaction	After reaction
Pd/SO_3H-MCM-41	0.40	0.32
Pd/SO_3H-MCM-48	0.36	0.32
Pd/SO_3H-MSU-1	0.43	0.39
Pd/SO_3H-SBA-15	0.41	0.36
Pd/SO_3H-MCF	0.38	0.34

Yield for hydrogen peroxide increased in the order of Pd/SO_3H-MCM-41 (7.3%) < Pd/SO_3H-MCM-48 (7.6%) < Pd/SO_3H-MSU-1 (11.6%) < Pd/SO_3H-SBA-15 (15.3%) < Pd/SO_3H-MCF (17.0%). Final concentration of hydrogen peroxide after a 6-h reaction also increased in the order of Pd/SO_3H-MCM-41 (0.30 wt%) < Pd/SO_3H-MCM-48 (0.37 wt%) < Pd/SO_3H-MSU-1 (0.57 wt%) < Pd/SO_3H-SBA-15 (0.66 wt%) < Pd/SO_3H-MCF (0.72 wt%). Among the catalysts tested, Pd/SO_3H-MCF showed the best catalytic performance.

As mentioned earlier, it is known that acid additives cause the dissolution of palladium species from the supported palladium catalyst [1,2]. In this work, therefore, SO_3H-functionalized mesoporous silica supports were utilized as an alternate acid source. As listed in Table 2, no significant dissolution of palladium species was observed in the Pd/SO_3H-functionalized mesoporous silicas before and after the reaction.

3.4. Catalytic performance in the hydrogenation of hydrogen peroxide

Fig. 11 shows the catalytic performance in the hydrogenation of hydrogen peroxide over Pd/mesoporous silicas (Pd/MCM-41, Pd/MCM-48, Pd/MSU-1, Pd/SBA-15, and Pd/MCF) and Pd/SO_3H-functionalized mesoporous silicas (Pd/SO_3H-MCM-41, Pd/SO_3H-MCM-48, Pd/SO_3H-MSU-1, Pd/SO_3H-SBA-15, and Pd/SO_3H-MCF). Pd/mesoporous silica catalysts showed high activity for hydrogenation of hydrogen peroxide. This indicates that the hydrogenation of hydrogen peroxide was activated over Pd/mesoporous silica catalyst. Pd/SO_3H-functionalized mesoporous silica catalysts also showed high activity for hydrogenation of hydrogen peroxide. These results indicate that the enhanced acid property of Pd/SO_3H-functionalized mesoporous silica catalysts exhibited no significant effect on the prevention of hydrogenation of hydrogen peroxide.

3.5. Catalytic performance in the decomposition of hydrogen peroxide

Fig. 12 shows the catalytic performance in the decomposition of hydrogen peroxide over Pd/mesoporous silicas (Pd/MCM-41, Pd/MCM-48, Pd/MSU-1, Pd/SBA-15, and Pd/MCF) and Pd/SO_3H-functionalized mesoporous silicas (Pd/SO_3H-MCM-41, Pd/SO_3H-MCM-48, Pd/SO_3H-MSU-1, Pd/SO_3H-SBA-15, and Pd/SO_3H-MCF). Activity for decomposition of hydrogen peroxide over Pd/SO_3H-functionalized mesoporous silica catalysts was much lower than that over Pd/mesoporous silica catalysts. This implies that the

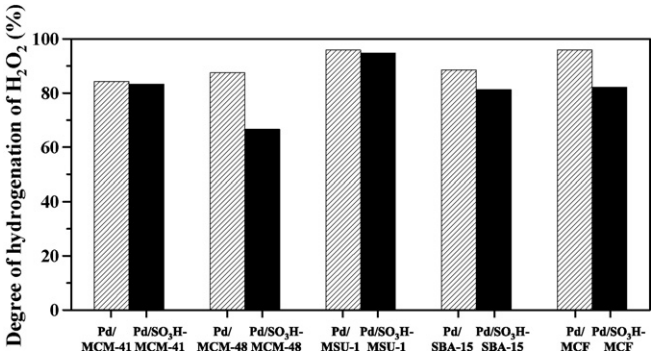

Fig. 11. Catalytic performance in the hydrogenation of hydrogen peroxide over Pd/mesoporous silicas (Pd/MCM-41, Pd/MCM-48, Pd/MSU-1, Pd/SBA-15, and Pd/MCF) and Pd/SO_3H-functionalized mesoporous silicas (Pd/SO_3H-MCM-41, Pd/SO_3H-MCM-48, Pd/SO_3H-MSU-1, Pd/SO_3H-SBA-15, and Pd/SO_3H-MCF).

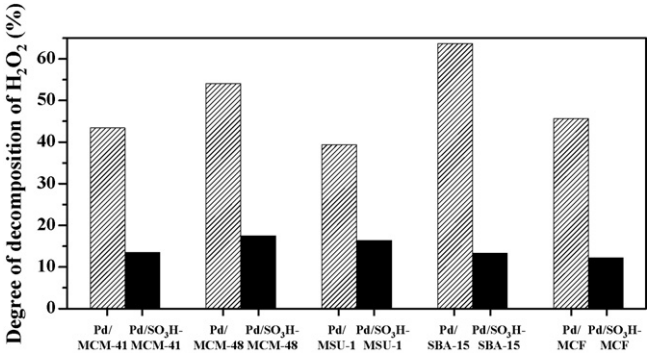

Fig. 12. Catalytic performance in the decomposition of hydrogen peroxide over Pd/mesoporous silicas (Pd/MCM-41, Pd/MCM-48, Pd/MSU-1, Pd/SBA-15, and Pd/MCF) and Pd/SO_3H-functionalized mesoporous silicas (Pd/SO_3H-MCM-41, Pd/SO_3H-MCM-48, Pd/SO_3H-MSU-1, Pd/SO_3H-SBA-15, and Pd/SO_3H-MCF).

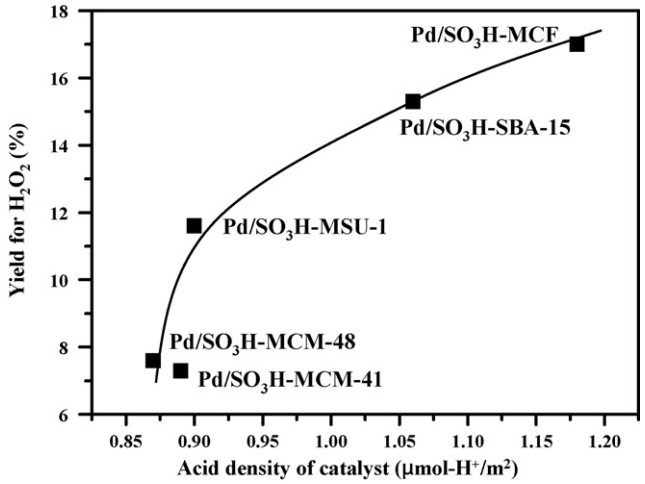

Fig. 13. A correlation between yield for hydrogen peroxide over Pd/SO_3H-functionalized mesoporous silicas (Pd/SO_3H-MCM-41, Pd/SO_3H-MCM-48, Pd/SO_3H-MSU-1, Pd/SO_3H-SBA-15, and Pd/SO_3H-MCF) and acid density of the catalysts.

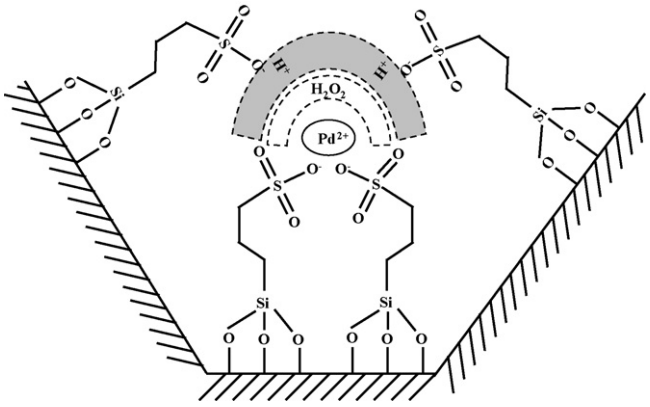

Fig. 14. Schematic presentation of effective surround of hydrogen peroxide by protons of Pd/SO_3H-functionalized mesoporous silica.

inhibited decomposition of hydrogen peroxide over Pd/SO_3H-functionalized mesoporous silica catalysts was attributed to the enhanced acid property of Pd/SO_3H-functionalized mesoporous silica catalysts, as reported in previous works [1,2]. These results support that Pd/SO_3H-functionalized mesoporous silica catalysts enhanced the selectivity for hydrogen peroxide by preventing the decomposition of hydrogen peroxide.

3.6. Effect of acid density on the catalytic performance

In order to elucidate the different catalytic performance of Pd/SO_3H-functionalized mesoporous silicas (Pd/SO_3H-MCM-41, Pd/SO_3H-MCM-48, Pd/SO_3H-MSU-1, Pd/SO_3H-SBA-15, and Pd/SO_3H-MCF), acid amount of Pd/SO_3H-functionalized mesoporous silicas was measured by an acid–base titration [33,34]. Acid density of Pd/SO_3H-functionalized mesoporous silicas was then calculated by dividing acid amount of Pd/SO_3H-functionalized mesoporous silicas by surface area of the catalysts. Acid amount of Pd/SO_3H-functionalized mesoporous silicas increased in the order of Pd/SO_3H-MCF = Pd/SO_3H-SBA-15 (0.54 mmol-H^+/g) < Pd/SO_3H-MSU-1 = Pd/SO_3H-MCM-41 (0.78 mmol-H^+/g) < Pd/SO_3H-MCM-48 (0.98 mmol-H^+/g). Acid density of Pd/SO_3H-functionalized mesoporous silicas increased in the order of Pd/SO_3H-MCM-48 (0.87 μmol-H^+/m^2) < Pd/SO_3H-MCM-41 (0.89 μmol-H^+/m^2) < Pd/SO_3H-MSU-1 (0.90 μmol-H^+/m^2) < Pd/SO_3H-SBA-15 (1.06 μmol-H^+/m^2) < Pd/SO_3H-MCF (1.18 μmol-H^+/m^2). Among the Pd/SO_3H-functionalized mesoporous silicas, Pd/SO_3H-MCF catalyst exhibited the highest acid density.

Experimental observations revealed that there was no reliable correlation between yield for hydrogen peroxide over Pd/SO_3H-functionalized mesoporous silicas and acid amount of the catalysts. However, yield for hydrogen peroxide over Pd/SO_3H-functionalized mesoporous silicas was closely related to the acid density of the catalysts (Fig. 13). Yield for hydrogen peroxide increased with increasing acid density of Pd/SO_3H-functionalized mesoporous silica. This implies that acid density of Pd/SO_3H-functionalized mesoporous silicas played an important role in determining the catalytic performance in the direct synthesis of hydrogen peroxide from hydrogen and oxygen. As mentioned earlier, it has been reported that acid additives prevent the decomposition of hydrogen peroxide because hydrogen peroxide is surrounded by protons of acid additives [1,2]. It is known that protons of acid additives are free to move in reaction medium. However, protons of Pd/SO_3H-functionalized mesoporous silicas are restricted to transfer in reaction medium. Therefore, effective surround of hydrogen peroxide by protons of Pd/SO_3H-functionalized mesoporous silicas is possible, when acid density (compactness of protons) of Pd/SO_3H-functionalized mesoporous silicas is sufficiently high (Fig. 14). Thus, acid density of Pd/SO_3H-functionalized mesoporous silicas served as a crucial factor determining the catalytic performance in the direct synthesis of hydrogen peroxide. Among the catalysts tested, Pd/SO_3H-MCF catalyst with the highest acid density showed the highest yield for hydrogen peroxide. This indicates that SO_3H-MCF served as an efficient acidic support in the direct synthesis of hydrogen peroxide from hydrogen and oxygen. It is concluded that the improved yield for hydrogen peroxide over Pd/SO_3H-functionalized mesoporous silicas was attributed to the enhanced acid density of the catalysts. Pd/SO_3H-functionalized mesoporous silicas efficiently served as an alternate acid source and as an active metal catalyst in the direct synthesis of hydrogen peroxide.

4. Conclusions

SO_3H-functionalized mesoporous silicas were prepared using MCM-41, MCM-48, MSU-1, SBA-15, and MCF. Pd/SO_3H-functionalized mesoporous silicas were then applied to the direct synthesis of hydrogen peroxide from hydrogen and oxygen. For comparison, Pd/mesoporous silicas were also employed for the direct synthesis of hydrogen peroxide. Selectivity for hydrogen peroxide, yield for hydrogen peroxide, and final concentration of hydrogen peroxide over Pd/SO_3H-functionalized mesoporous silica catalysts were much higher than those over Pd/mesoporous silica catalysts. Thus, Pd/SO_3H-functionalized mesoporous silicas served as efficient catalysts in the direct synthesis of hydrogen peroxide. High catalytic performance of Pd/SO_3H-functionalized mesoporous silicas was attributed to the enhanced acid property of the catalysts. It was revealed that yield for hydrogen peroxide increased with increasing acid density of Pd/SO_3H-functionalized mesoporous silica. Among the catalysts tested, Pd/SO_3H-MCF catalyst with the highest acid density showed the highest yield for hydrogen peroxide.

Acknowledgements

This work was financially supported by the grant from the Industrial Source Technology Development Programs (10033093) of the Ministry of Knowledge Economy (MKE) of Korea.

References

[1] J.M. Campos-Martin, G. Blanco-Brieva, J.L.G. Fierro, Angew. Chem. Int. Ed. 45 (2006) 6962–6984.
[2] C. Samanta, Appl. Catal. A 350 (2008) 133–149.
[3] S. Park, K.M. Cho, M.H. Youn, J.G. Seo, J.C. Jung, S.-H. Baeck, T.J. Kim, Y.-M. Chung, S.-H. Oh, I.K. Song, Catal. Commun. 9 (2008) 2485–2488.
[4] J.H. Lunsford, J. Catal. 216 (2003) 455–460.
[5] S. Chinta, J.H. Lunsford, J. Catal. 225 (2004) 249–255.
[6] V.R. Choudhary, C. Samanta, T.V. Choudhary, Appl. Catal. A 308 (2006) 128–133.
[7] V.R. Choudhary, C. Samanta, J. Catal. 238 (2006) 28–38.
[8] V.R. Choudhary, P. Jana, J. Catal. 246 (2007) 434–439.
[9] C. Samanta, V.R. Choudhary, Catal. Commun. 8 (2007) 73–79.
[10] Y.-F. Han, J.H. Lunsford, Catal. Lett. 99 (2005) 13–19.
[11] Y.-F. Han, J.H. Lunsford, J. Catal. 230 (2005) 313–316.
[12] G. Li, J. Edwards, A.F. Carley, G.J. Hutchings, Catal. Commun. 8 (2007) 247–250.
[13] P. Landon, P.J. Collier, A.J. Papworth, C.J. Kiely, G.J. Hutchings, Chem. Commun. (2002) 2058–2059.
[14] J.K. Edwards, B.E. Solsona, P. Landon, A.F. Carley, A. Herzing, C.J. Kiely, G.J. Hutchings, J. Catal. 236 (2005) 69–79.
[15] J.K. Edwards, A. Thomas, A.F. Carley, A.A. Herzing, C.J. Kiely, G.J. Hutchings, Green Chem. 10 (2008) 388–394.
[16] G. Bernardotto, F. Menegazzo, F. Pinna, M. Signoretto, G. Cruciani, G. Strukul, Appl. Catal. A 358 (2009) 129–135.
[17] Q. Liu, J.C. Bauer, R.E. Schaak, J.H. Lunsford, Appl. Catal. A 339 (2008) 130–136.
[18] S. Park, S.H. Lee, S.H. Song, D.R. Park, S.-H. Baeck, T.J. Kim, Y.-M. Chung, S.-H. Oh, I.K. Song, Catal. Commun. 10 (2009) 391–394.
[19] S. Melada, R. Rioda, F. Menegazzo, F. Pinna, G. Strukul, J. Catal. 239 (2006) 422–430.
[20] S. Park, J.C. Jung, J.G. Seo, T.J. Kim, Y.-M. Chung, S.-H. Oh, I.K. Song, Catal. Lett. 130 (2009) 604–607.
[21] S. Park, T.J. Kim, Y.-M. Chung, S.-H. Oh, I.K. Song, Catal. Lett. 130 (2009) 296–300.
[22] W.M. Van Rhijn, D.E. De Vos, B.F. Sels, W.D. Bossaert, P.A. Jacobs, Chem. Commun. (1998) 317–318.
[23] D. Das, J.-F. Lee, S. Cheng, J. Catal. 223 (2004) 152–160.
[24] O. de la Iglesia, M. Pedernera, R. Mallada, Z. Lin, J. Rocha, J. Coronas, J. Santamaría, J. Membr. Sci. 280 (2006) 867–875.
[25] D. Kumar, K. Schumacher, C. du Fresne von Hohenesche, M. Grün, K.K. Unger, Colloids Surf. A 187–188 (2001) 109–116.
[26] C. Boissière, A. Larbot, A. van der Lee, P.J. Kooyman, E. Prouzet, Chem. Mater. 12 (2000) 2902–2913.
[27] D. Zhao, J. Feng, Q. Huo, N. Melosh, G.H. Fredrickson, B.F. Chmelka, G.D. Stucky, Science 279 (1998) 548–552.
[28] K. Kannan, R.V. Jasra, J. Mol. Catal. B 56 (2009) 34–40.
[29] P. Schmidt-Winkel, W.W. Lukens Jr., P. Yang, D.I. Margolese, J.S. Lettow, J.Y. Ying, G.D. Stucky, Chem. Mater. 12 (2000) 686–696.
[30] Q. Yang, M.P. Kapoor, S. Inagaki, N. Shirokura, J.N. Kondo, K. Domen, J. Mol. Catal. A 230 (2005) 85–89.
[31] Q. Yang, J. Liu, J. Yang, M.P. Kapoor, S. Inagaki, C. Li, J. Catal. 228 (2004) 265–272.
[32] D. Margolese, J.A. Melero, S.C. Christiansen, B.F. Chmelka, G.D. Stucky, Chem. Mater. 12 (2000) 2448–2459.
[33] B. Rác, Á. Molnár, P. Forgo, M. Mohai, I. Bertóti, J. Mol. Catal. A 244 (2006) 46–57.
[34] I.J. Dijs, H.L.F. van Ochten, A.J.M. van der Heijden, J.W. Geus, L.W. Jenneskens, Appl. Catal. A 241 (2003) 185–203.
[35] R.M. Hanson, K.B. Sharpless, J. Org. Chem. 51 (1986) 1922–1925.
[36] C. Pak, G.L. Haller, Micropor. Mesopor. Mater. 48 (2001) 165–170.
[37] S. Shylesh, S. Sharma, S.P. Mirajkar, A.P. Singh, J. Mol. Catal. A 212 (2004) 219–228.